



# J C M M

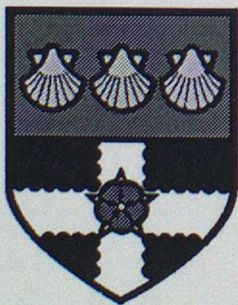
**Observations of stratospheric air  
entering the circulation of a polar low**

**K A Browning  
and  
E M Dicks**

**May 2000**

**INTERNAL REPORT NO.113**

*NWP Technical Report No.307*



**Joint Centre for Mesoscale Meteorology**

Observations of stratospheric air entering the circulation of a polar low

K.A.Browning\* and E.M.Dicks

Joint Centre for Mesoscale Meteorology, University of Reading, UK

Summary

Dry air descending within the circulation of a polar low was observed to give a striking signature in the echo return from an upward-looking VHF radar. Data from this radar, along with weather radar data, satellite imagery and output from limited-area and mesoscale versions of the Met Office Unified Model, are synthesized to depict the mesoscale structure of the weather system. The polar low had a compact vortex centred near 3 km, a cold core below this level and a warm core above. Attribution of quasi-geostrophic forcing showed that on the larger scale the polar low was dominated by upper-level forcing. The detailed mesoscale analysis showed that the polar low, during its mature phase, was affected by a stratospheric intrusion that brought air from near tropopause level down to 3 km to give the striking signature in the VHF radar echo pattern. The echo pattern also suggested that thin tongues of this stratospheric, or near-stratospheric, air were penetrating slantwise down a further several hundred metres into the shallow cloud constituting the southern end of an archetypal cloud head. It is argued that this was a locally important region of mixing between air originating near the tropopause and the boundary layer. In more general terms, the study demonstrates the ability of the operational mesoscale model to represent various small-scale features. The study also helps in developing the interpretation of the patterns of clear-air radar echo observed with VHF radar.

---

\* Corresponding author: Joint Centre for Mesoscale Meteorology, Department of Meteorology, University of Reading, PO Box 243, Reading, RG6 6BB

## 1. Introduction

Polar lows are mesoscale phenomena of both scientific and practical significance. Their practical importance arises from the locally heavy snowfalls and strong winds they can produce and the difficulty in forecasting them. Their scientific interest as a topic of continuing research is kept alive by their elusive nature which tends to inhibit a good description and understanding of them. It is particularly difficult to obtain mesoscale observations of polar lows not only because they are small and rather infrequent but also because they occur mainly over poorly instrumented ocean areas. Once in a while, however, they pass close to relatively well observed coastal regions thereby enabling a more detailed mesoanalysis to be undertaken (eg Hewson et al 2000).

Recently, in Easter 1998, an intense polar low travelled southwards down the Irish Sea, giving 15cm of snow at Ronaldsway Airport (L.A.Hisscott, pers.comm.) and passing close to the MST (Mesosphere-Stratosphere-Troposphere) radar at Aberystwyth (Slater et al 1991). This VHF radar system provided continuous vertical soundings of wind and echo power (from which regions of strong humidity gradients and/or static stability can be inferred) and this enabled a very detailed analysis to be carried out during the passage of the polar low. The Easter 1998 polar low also passed close to three radiosonde stations as well as many surface stations. Operational runs of the mesoscale (17 km grid) version of the UK Met Office's Unified Model (Cullen 1993) on 14 April, benefiting from assimilation of the relatively plentiful local data, were found to represent detailed aspects of its structure that conformed well to the structure inferred from the VHF radar. The present study exploits this rather rare observational opportunity to reveal some interesting features of the mesoscale structure of the polar low. It also provides a good opportunity to deepen our appreciation of the interpretation of the data obtained from VHF radar.

There is much variability in the nature of polar lows, arising in part from differing combinations of baroclinic and convective activity (Bader et al 1995). Although there was some shallow convective activity in the present case, this event appeared to be strongly affected by slantwise ascent, with most of the snow occurring in a region of rather uniform precipitation associated with a cloud head (see Sec.2). The polar low was located on the edge of a cold-air dome but the minimum temperature ( $-40^{\circ}\text{C}$ ) in the centre of the dome at 500 mb was not quite low enough for the low to be referred to as a primary polar low according to the classification of Rasmussen et al (1993). The most striking feature of this case was the pronounced dry intrusion (Browning 1997) associated with the descent of stratospheric air within the circulation of the polar low. This has been well documented for this case and forms the main theme of the study.

## 2. Synoptic overview

The polar low on 14 April 1998 was accompanied by a well defined mesoscale cloud head and polar-front cloud band. Its structure was a mesoscale version of the larger archetypal extra-tropical cyclone structure as described in reviews by Bader et al (1991) and Browning (1999), a fact also noted by Hewson et al (2000) for other polar lows. Figure 1 shows the associated distribution of cloud and low-level precipitation at 09 and 15 UTC as the centre of the polar low (L) travelled south-eastwards down the northern Irish Sea. The mesoscale polar-front cloud band is highlighted by the analysed surface cold front and the convex outer edge of the cloud head is highlighted by the wavy line. A narrow band of precipitation can be seen along the cold front but most of the precipitation, mainly snow, is associated with the cloud head in the region of slantwise ascent on the poleward side of the surface warm front. For the most part, the precipitation stops short of the outer edge of the cloud head because of evaporation below cloud base. Also shown in Fig. 1 (line with open cold frontal symbols) is an upper-level dry front (cold wet-bulb potential temperature front) associated with very dry air overrunning part of the cloud head from the north. The position of this dry front was inferred, as discussed later in Sec 3, from the leading edge of dry air seen in

the satellite water vapour imagery. This dry air was associated with the stratospheric intrusion that constitutes the main theme of this paper.

As will become clear from a number of comparisons with observations made throughout this paper, the analyses and (T+3) forecasts from the operational mesoscale model successfully represented many aspects of the detailed structure of the polar low. An overview of the structure of the polar low obtained from the mesoscale model at 15 UTC is given in Fig 2. Figure 2(a) shows the surface analysis. The superimposed pattern of model-derived precipitation agrees broadly with the radar observations in Fig.1(b). Much of the snow associated with the cloud head was due to large-scale (resolved) ascent. Convective precipitation was diagnosed, especially along the cold front (and in other regions unrelated to the polar low). Figure 2(b) shows the distribution of the southerly component of the wind at the level (800 mb) of maximum vorticity. Note the dipole near the North Wales coast where a  $26 \text{ ms}^{-1}$  change ( $-18$  to  $+8 \text{ m s}^{-1}$ ) occurs over a distance of just over 100 km in association with the compact vortex core centred near this level.

Figures 2(c) and 2(d) show the wet-bulb potential temperature ( $\theta_w$ ) at 900 and 600 mb, respectively. The dashed lines sketched in Fig. 2(c) draw attention to axes of high and low  $\theta_w$  corresponding to mesoscale versions of warm-conveyor-belt (WCB) and cold-conveyor-belt (CCB) flows. The mesoscale WCB is characterised by  $\theta_w \sim 276\text{-}277\text{K}$  and is traceable approaching the low centre at 800 and 700 mb (not shown), culminating in a cut-off warm core at 600 mb as shown by the letter W in Fig. 2(d). The axis of the mesoscale CCB ( $\theta_w \sim 273\text{-}274\text{K}$ ) is situated at 900 mb beneath the outer edge of the cloud head and culminates within the southern tip of the cloud head beneath where stratospheric air descends to about 700 mb (3km) (see later Sections 3 and 4).

On a broader scale, it is instructive to examine the field of quasi-geostrophic vertical velocity from the Limited Area version of the Unified Model (50 km grid spacing) to establish the nature of the forcing of vertical velocity in the region of the polar low. We use a diagnostic developed by Clough and Davitt (1994) to represent the quasi-geostrophic vertical velocity ( $W_{QG}$ ) attributable to forcing from different levels. Figures 3(a) and 3(b) depict fields of 700 mb  $W_{QG}$  at 12UTC, attributable to forcing from (a) upper levels (650-50mb) and (b) lower levels (1050-750mb). These figures show that the  $W_{QG}$  dipole has a scale of 900 km due to upper-level forcing and 300 km due to lower-level forcing, that there is ascent forced from both levels at the location of the polar low (in the Northern Irish Sea close to the Isle of Man), and that the forcing from the upper levels is dominant (even allowing for the fact that the upper layer as defined is deeper than the lower layer). Figure 4 depicts the evolution of the maxima and minima in both the upper- and lower-level  $W_{QG}$  dipoles from 12 UTC on 13 April to 21 UTC on 14 April. It shows that not only does the magnitude of the forcing increase with time (along with the maximum vorticity at 900 mb) but also that the upper-level forcing dominates by an order of magnitude throughout the period. During the latter part of the period depicted in Fig.4, an intrusion of stratospheric air descended within the circulation of the polar low, reaching 700 mb (3km) at 18 UTC. We examine this behaviour in the next section.

### 3. The stratospheric intrusion

Areas of high brightness temperature, so-called dark zones in conventional black-&-white satellite water vapour imagery, correspond to pockets of dry air at upper levels (Weldon and Holmes 1991). They can be used to identify the tropopause depressions which often form in the vicinity of cyclones (Mansfield 1996,1997). When the base of these tropopause depressions lowers, often accompanied by tropopause folding, the size and darkness of these zones increases. Such a behaviour was evident for the polar low on 14 April. Figure 5 shows a sequence of images from 0930 to

1830 UTC during which period a dark zone appeared over the North Channel between Scotland and Ireland and then travelled southwards toward Wales, intensifying as it went. The series of solid lines shown later in Fig.6(d) depicts the successive positions of the leading edge of the dark zone. This is the upper-level dry front that was plotted in Figs. 1(a) and (b). The dotted lines in Fig.6(d), drawing attention to the outer edge of the cloud head, show that the dry air straddles part of the cloud head.

Evidence that the dry air identified by the dark zone in the WV imagery was indeed stratospheric air is provided by comparing the imagery with the pattern of potential vorticity (PV) derived from the mesoscale model. Figure 6(a) depicts the 3-dimensional structure of the dynamic tropopause ( $PV = 2$ )\* at 15 UTC. It shows the  $PV = 2$  surface extending from a broad trough at 400 mb down into a tropopause depression at 500 mb centred over the northeast coast of Ireland. The 500 mb tropopause depression travelled southwards and Fig. 6(b) shows the  $PV = 2.4$  contour growing in a manner that resembles the behaviour of the WV dark zone in Figs. 5 and 6(d). At lower levels, Fig. 6(a) shows that near-stratospheric air with  $PV = 1.4$  extends southwestwards within a narrow tropopause fold just behind of the surface cold front (Fig. 1). Figure 6(c) shows the lowermost tip of the tropopause fold at 600 mb travelling south-southeastwards. By 18 UTC, the eastern end of the tip of the tropopause fold passed close to Aberystwyth (A) and Aberporth ( $A_1$ ). This is consistent with the VHF radar data presented in Sec.4.

Radiosondes were launched every 6 hours from Aberporth. The sonde released at 12 UTC on 14 April (Fig. 7(a)) shows the primary tropopause (T1) at about 330 mb (8.5 km), with evidence of a weak fold down to 550 mb (T2). The 18 UTC sonde (Fig. 7(b)) shows very dry stratospheric or near-stratospheric air down to 650 mb in association with the passage of the main tropopause fold. As is often the case in such a region, there is no clearly

---

\* Units of PV are  $10^{-6} \text{ m}^2 \text{ s}^{-1} \text{ K kg}^{-1}$

defined tropopause within the temperature profile in Fig. 7(b). Further details about the structure of this tropopause fold can be gleaned by examining time-height sections from the model and VHF radar at nearby Aberystwyth.

#### 4. Time-height sections over Aberystwyth

The VHF radar at Aberystwyth was well positioned to observe the passage of the lowermost penetration of the stratospheric air. To guide our interpretation of the radar data, we first show model-derived time-height sections of potential vorticity (PV) (Fig. 8(a)) and relative humidity (Fig. 8(b)) for the model grid point nearest Aberystwyth. Both Figs. 8(a) and 8(b) show features indicative of the deep penetration of the stratospheric air. The stratospheric, or near-stratospheric, air comes down in two folds: at 14 UTC and at 18 UTC. At 14 UTC the PV = 1.5 contour steps down from 8 to 6 km and at 18 UTC it steps down from 5 to 3½ km (Fig. 8(a)). Tongues of low (25%) RH within the folds get down to 6 km after 14 UTC for the first fold and to 3½ km after 18 UTC for the second fold (Fig. 8(b)). The nearby 12 UTC sounding at Aberporth (Fig. 7(a)) shows the main tropopause (T1) at 8.5 km and the base of the dry stable layer (T2) associated with the first fold at 5 km. At the time of the 18 UTC Aberporth sounding (Fig. 7(b)), Figs. 8 (a) and (b) show that the second, and principal, tropopause fold has brought air with PV = 1.5 and RH = 20% down to about 3½ km and there is a tendency, from 16 to 18 UTC, for the dry air (with low  $\theta_w$ ) to undercut the moist (WCB) air (with relatively high  $\theta_w$ ) ahead of it.

The time-height sections from the VHF radar are shown in Fig. 9. Figure 9(a) shows echo power, (b) shows wind direction and (c) shows wind strength (superimposed on (b) and (c) are mesoscale-model-derived values to indicate the broadly good performance of the model). The pattern of echo in Fig. 9(a) can be related to the patterns of PV and RH in Figs. 8(a) and (b): in particular, the red layer corresponding to strong radar signal marks the lower

boundary of the dry air, initially at 5 km in association with the first tropopause fold, and then, between 1730 and 1930 UTC, at 3 km in association with the deep intrusion of stratospheric air related to the second and principal tropopause fold. The inclined isopleths of wind direction below 4km from 17 to 20 UTC, in Fig. 9(b), are associated with the passage of the rearward-sloping zone of maximum vorticity characterising this deep stratospheric intrusion. The relationship between this mesoscale vortex and the lower boundary of the dry air is summarized in Fig. 10.

The rearward-sloping maxima in wind-strength (ie orange features sloping downwards from left to right) below 4 km between 1630 and 17 UTC in Fig. 9(c) are collocated and parallel to spikes of high echo-power (orange and red) in Fig. 9(a); these spikes are believed to correspond to the edges of deeply penetrating narrow tongues of dry stratospheric or near-stratospheric air bounding the regions of ascent highlighted by the 2 narrower arrows sketched in Fig. 10. These regions of ascent were associated with the rear half of the cold-frontal cloud band evident in the satellite imagery in Figs. 11(a) and (b). This part of the cold-frontal cloud band produced very little precipitation. However, the part of the cold-frontal cloud band which passed over Aberystwyth between 16 and 1630 UTC produced a narrow band of heavy precipitation. The region of ascent responsible for this precipitation, shown by the broadest of the three arrows in Fig. 10, was associated with the rearward-sloping column of relatively weak radar echo below 3 km, shown green in Fig.9(a). Based on a system velocity of  $33 \text{ km h}^{-1}$ , the slope of these features is roughly 1 vertically in 5 horizontally. The model (Fig.2(a)) suggests that this is a region of mixed slantwise and upright convection. The pattern of relative humidity in Fig.8(b) and of  $\theta_w$  (not shown) is consistent with a rearward-sloping (ie ana) cold front.

The deepest downward penetration of dry stratospheric or near-stratospheric air was that which descended slantwise from 3 km at 1730 UTC

to below  $2\frac{1}{2}$  km just after 1720 UTC (Fig. 10). This corresponded to a narrow break in the cloud which was associated with the dark strip just behind the polar-front cloud band seen approaching Aberystwyth at 1700 UTC in the satellite images in Figs. 11(a) and (b). Immediately following this dark strip in the imagery, the next cloud feature to pass over Aberystwyth was the shallow southern tip of the cloud head (i.e. the part extending to the south of the extreme north-western tip of Wales). The visible image shows that the cloud tops here have a fingered structure, believed to be related to the small undulations in the lower limit of the stratospheric intrusion as identified in the intense VHF radar echo layer seen in Fig. 9(a) (and Fig.10) between 1730 and 1930 UTC. The radiosonde ascent in Fig. 7(b) shows that this cloud was associated with air that would have ascended convectively (slantwise and/or upright) from near the surface of the relatively warm sea. An analysis of an enhanced version of the infrared image shows that the brightness temperatures in this region were consistent with the cloud tops being below about  $1\frac{1}{2}$  km assuming an emissivity of unity. The apparent discrepancy between the inferred cloud-top height and the radar-detected dry-air boundary may be due to the clouds having a low emissivity. This would be consistent with the likely presence of ice in these clouds and the absence of particles large enough to be detected by the weather radar network (see Fig.1(b))

#### 4. Concluding remarks

A rare opportunity to study the mesoscale structure of a polar low arose on 14 April 1998 when a small polar low passed almost overhead of the VHF research radar at Aberystwyth. An analysis of data from this radar and several other sources, including the Limited-Area and mesoscale versions of the Met Office's operational NWP model, showed that the polar low was dominated by upper-level forcing and that stratospheric air, or near-stratospheric air, descended down to about 3 km over an area of order 100 km across. The sketch in Fig. 10, depicting the interface between this

stratospheric intrusion and the underlying moist air, shows two regions distinct regions. The first region (before 1720 UTC) is associated with the passage of the mesoscale cold front and associated cloud band: here mesoscale warm-conveyor-belt flows ascend rearwards into the dry air in a number of plumes rising up to 4½ km. The second region, after the passage of the cold front, is where the stratospheric intrusion descends broadly down to 3 km above the southern tip of the cloud head. The top of the cloud head had a finely fingered structure owing to interpenetrating layers of slantwise ascent and descent.

The situation described above is believed to have been almost identical to that observed in a somewhat larger-scale cyclone by Browning et al (1995; see their Section 5). By using closely spaced dropsondes, they showed that individual interpenetrating layers of air extended slantwise over a large fraction of the 3 km-deep moist layer at the southern tip of a cloud head. As shown in Browning (1999; see Fig.17) the vertical wind shear between these same interpenetrating flows was strong enough for shearing instability to develop. In our experience, fingered structures in the low cloud are common near the southern tip of cloud heads and incipient cloud heads. The slantwise interpenetrating flows that they imply may represent a locally significant mechanism for mixing lower-stratospheric and upper-tropospheric air down into the boundary layer.

#### Acknowledgements

The Joint Centre for Mesoscale Meteorology is supported by the Meteorological Office and the Department of Meteorology, University of Reading. The research was undertaken under the auspices of the Universities Weather Research Network (UWERN) funded by the Natural Environment Research Council. We are grateful to the Met Office for giving access to radar, satellite and Unified Model data and for providing support for

wind profiler research. We thank Ken Slater and the British Atmospheric Data Centre for provision of data from the VHF radar and Gavin Winter for assistance in data processing. We also thank Peter Panagi and Tim Oakley for accessing the data and Abigail Deveson for generating Figs. 3 and 4.

### References

Bader, M.J., Forbes, G.S., Grant, J.R., Lilley, R.B.E and Waters, A.J. 1995 *Images in weather forecasting*. Cambridge University Press., pp 499.

Browning K.A. 1999 Mesoscale aspects of extratropical cyclones: an observational perspective. Pp 265-283 in *'The Life Cycles of Extratropical cyclones'*. (eds. M.A.Shapiro and S. Grønås), Amer.Meteorol.Soc.

Browning, K.A., Clough, S.A., Davitt, C.S.A, Roberts, N.M., Hewson T.D and Healey, P.G.W. 1995: Observations of the mesoscale sub-structure in the cold air of a developing frontal cyclone, *Q.J.R.Meteorol.Soc.*, **121**,1229-1254.

Clough, S.A. and Davitt, C.S.A. 1994 Development of an Atlantic frontal wave during IOP 3 of Fronts 92.Pp 151-156 in *'The Life Cycles of Extratropical Cyclones'*. Proceedings of an International Symposium, Geophysical Institute, University of Bergen, 27<sup>th</sup> June – 1<sup>st</sup> July 1994, (eds. S. Grønås and M.A.Shapiro) vol.II.

Cullen, M.J.B., 1993 The unified forecast/climate model, *Meteorol.Mag.*, **122**, 89-94.

Hewson, T.D., Craig, G.C. and Claud, C. 2000: Evolution and mesoscale structures of a polar low outbreak. *Q.R.J.Meteorol.Soc.*, **126**, 1031-1063.

Mansfield, D.A. 1996 The use of potential vorticity as an operational forecast tool. *Meteorol. Appl.*, **3**, 195-210.

Mansfield, D.A. 1997 The use of potential vorticity and water vapour imagery to validate numerical models. *Meteorol. Appl.*, **4**, 305-309

Rasmussen, E.A., Turner, J. and Twitchell, P.F. 1993 Report of a workshop on applications of new forms of satellite data in polar low research. *Bull. Amer. Meteorol. Soc.*, **74**, 1057-1073

Slater, K., Stevens, A.D., Pearman, S.A.M., Eccles, D., Hall, A.J., Bennett, R.G.T., France, L., Roberts, G., Olewicz, Z.K. and Thomas, L. 1991 Overview of the MST radar system at Aberystwyth, Pp 479-482 in Proceedings of the fifth workshop on technical and scientific aspects of MST radar. Ed. B. Edwards. SCOSTEP, Univ. of Illinois, Urbana, USA.

Weldon, R.B. and Holmes, S.J. 1991 Water vapour imagery, interpretation and applications to weather analysis and forecasting. *NOAA Tech Report NESDIS 57*, 213pp

## Figure Legends

- Fig. 1. Cloud and precipitation distributions at (a) 09 UTC and (b) 15 UTC, 14 April 1998. Grey shades represent brightness temperature from Meteosat infrared imagery (scale on right side of (a)). Colours represent equivalent rainfall rates from weather radar network (scale on right side of (b)). Overlays are explained in text.
- Fig. 2. Mesoscale model (T+3) forecast products valid at 15 UTC, 14 April 1998: (a) mean sea-level pressure (isobars every 1mb) and surface precipitation (horizontal hatching for precipitation due to resolved slantwise ascent and grey shading for that due to parametrised convection), (b) southerly wind component at 800 mb (isotachs every  $2 \text{ m s}^{-1}$ ) (c)  $\theta_w$  at 900 mb (isopleths every 1K, shading for  $< 274\text{K}$ ), and (d)  $\theta_w$  at 600 mb (isopleths every 0.5K; note the warm core labelled W). Analysed surface fronts have been added in (a) and (c) See text for explanation of dashed lines in (c).
- Fig. 3. Quasi-geostrophic vertical velocity  $W_{QG}$  at 700 mb attributable to (a) upper-level forcing and (b) low-level forcing, derived from the 50 km-grid Limited-Area Model T+3 forecast for 09 UTC, 14 April 1998. Solid (dashed) isopleths represent ascent (descent) at intervals of (a)  $0.2 \text{ cm s}^{-1}$  and (b)  $0.022 \text{ cm s}^{-1}$ , respectively. The polar low was situated in the Irish Sea over the Isle of Man at this time.
- Fig. 4. Time evolution of quasi-geostrophic vertical velocity ( $W_{QG}$ ) parameters derived from a sequence of charts like Fig. 3 during the development of the polar low on 13 and 14 April 1998. The solid and dashed curves show the magnitude (without regard to sign) of the maximum

(solid) and minimum (dashed) values of  $W_{QG}$  due to upper-level forcing (top two curves) and lower-level forcing (bottom two curves). The bold dotted curve shows the maximum value of relative vorticity at 900 mb for the resulting polar low. All curves are based on 6-hourly analyses and 6-hourly T+3 forecasts, and they have been smoothed to eliminate oscillations between analyses and forecasts.

Fig.5. Meteosat water-vapour imagery for (a) 0930 UTC, (b) 1230 UTC, (c) 1530 UTC and (d) 1830 UTC, 14 April 1998, using a compressed grey scale (229.5K, white, to 244.5K, black) to emphasise the dark zone. The white line and black dots along latitude 55.5°N in (b) are artefacts

Fig.6 Potential-vorticity plots from mesoscale model (a-c) for comparison with information from WV imagery in (d). (a) 3-D structure at 15 UTC and (b), (c) evolution of tropopause depression/fold from 9 to 18 UTC on 14 April 1998. (a) PV = 2 (standard units) at 400 mb (dashed contour) and 500 mb (thick solid contour) and PV = 1.4 at 600 mb (thin solid contour), all at 15 UTC (T+3). (b) PV = 2.4 at 500 mb and (c) PV at 600 mb at 09 UTC (grey shading), 12 UTC (T+0) (horizontal hatching) 15 UTC (T+3) (grey shading) and 18 UTC (T+0) (vertical hatching). The crosses in (c) labelled A and A<sub>1</sub> show the locations of Aberystwyth and Aberporth. (d) leading edge of dark zone (dry air) in Meteosat WV imagery at 0930, 1230, 1530 and 1830 UTC (solid lines), Dotted lines correspond to outer edge of part of cloud head as seen in WV imagery.

Fig.7. Tephigrams for Aberporth soundings at (a) 12 UTC and (b) 18 UTC, 14 April 1998. Points T1 and T2 in (a) are also labelled in Fig. 9(a).

Fig. 8. Time-height plots for Aberystwyth from 11 to 23 UTC, 14 April 1998: (a) potential vorticity and (b) relative humidity (with respect to ice),

derived from successive 6-hour runs of the mesoscale model starting at 06, 12 and 18 UTC. Grey scale for PV ranges from white ( $< 0$  PV units) to black ( $> 2$  PV units); isopleths are at intervals of 0.25 PV units. Grey scale for RH ranges from white (100%) to black (0%); isopleths are at intervals of 10%. The intrusion of dry air descending to low levels between 19 and 17 UTC in (b) is within a similarly sloping frontal zone (not shown) which reaches the ground as a surface cold front just after 15 UTC.

Fig.9. Time-height plots from 11 to 23 UTC, 14 April 1998, derived from the VHF radar at Aberystwyth: (a) radar power (colour scale in 5 dB steps; T1 and T2 refer to features in Fig.7(a)), (b) wind direction (colour scale in 10 deg steps from  $240^\circ$  to  $360^\circ$ ), and (c) wind strength (colour scale in  $2 \text{ m s}^{-1}$  steps from 0 to  $32 \text{ m s}^{-1}$ ). The black region below 1.7km is below the level of useable radar data. White contours superimposed on (b) and (c) show mesoscale-model-derived values (contours at 10 deg and  $2 \text{ m s}^{-1}$  intervals, respectively; the illegible bunched contours after 21 UTC in (b) are where the wind backs rapidly).

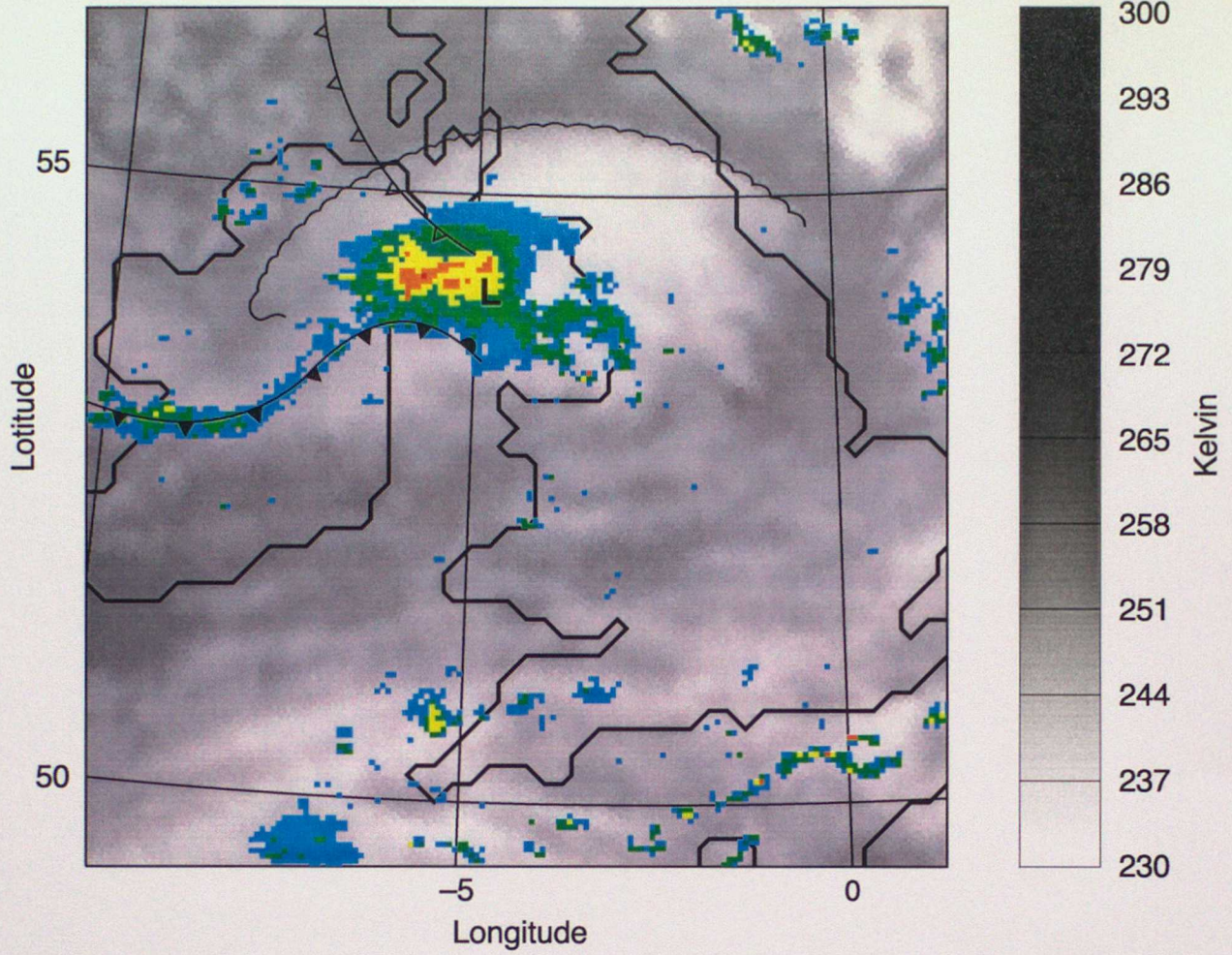
Fig.10. Summary time-height diagram of interface between the dry air of stratospheric or near-stratospheric origin and moist air originating in the boundary layer. The interface is represented by the thin wavy line superimposed on the region of high echo power shown as a grey-scale version of (part of) Fig.9(a). The intrusion of stratospheric air (and the air just below it) was associated with the western edge of a mesoscale vortex represented by the 4 dashed lines (corresponding to wind directions  $260^\circ$ ,  $280^\circ$ ,  $300^\circ$  and  $320^\circ$ ) which are linked by curved lines to create the impression of an inclined cylinder of recently descended air. The bold open arrows represent regions of warm high- $\theta_w$  air ascending rearwards which are responsible for the cold-frontal bands of cloud and precipitation. Air beneath the stratospheric

intrusion forms part of the southern tip of the cloud head. The black region below 1.7 km is below the level of useable VHF radar data..

Fig. 11. Meteosat imagery for 17 UTC, 14 April 1998: (a) infrared; (b) visible.

(a)

09 UTC



(b)

15 UTC

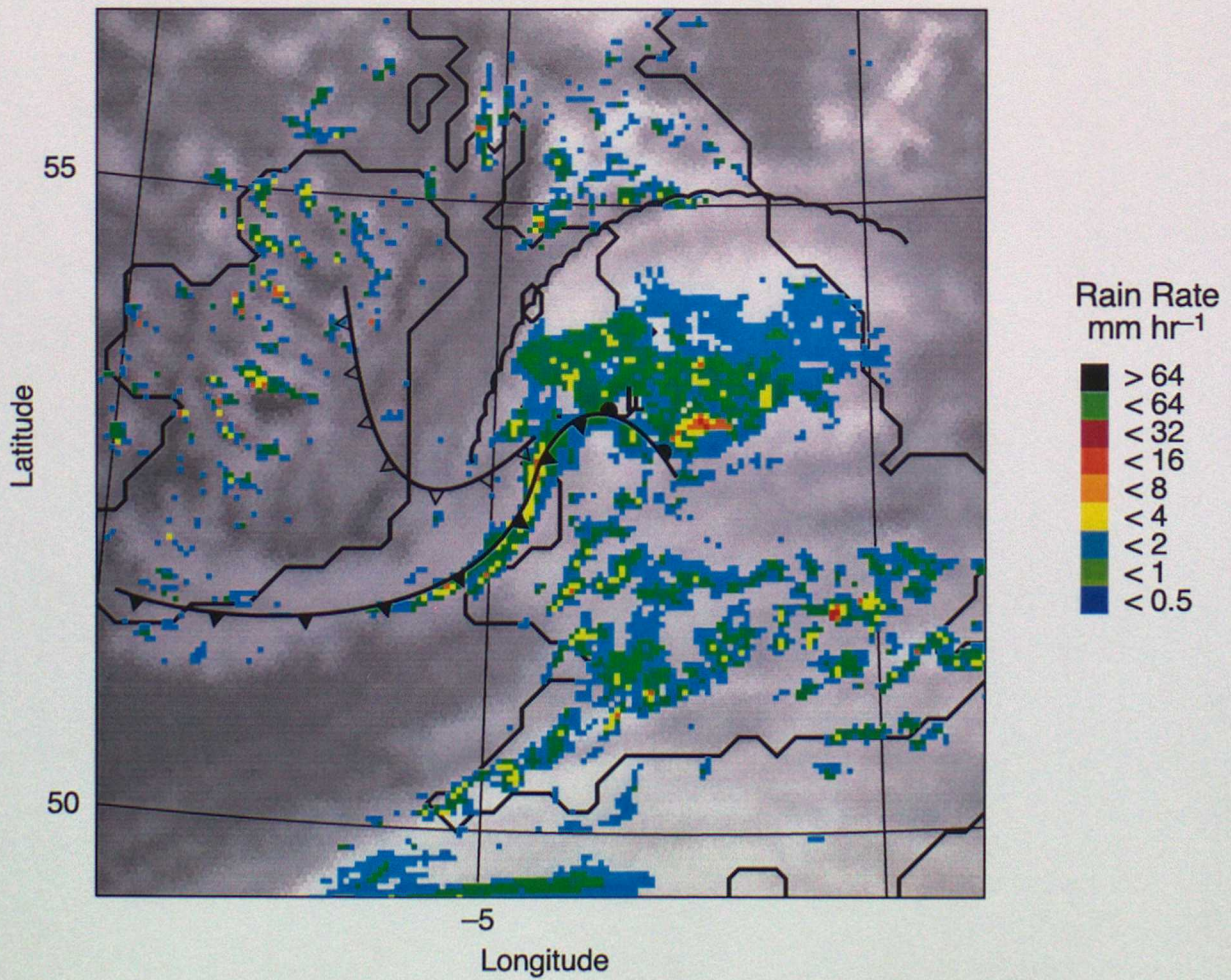


Fig 1

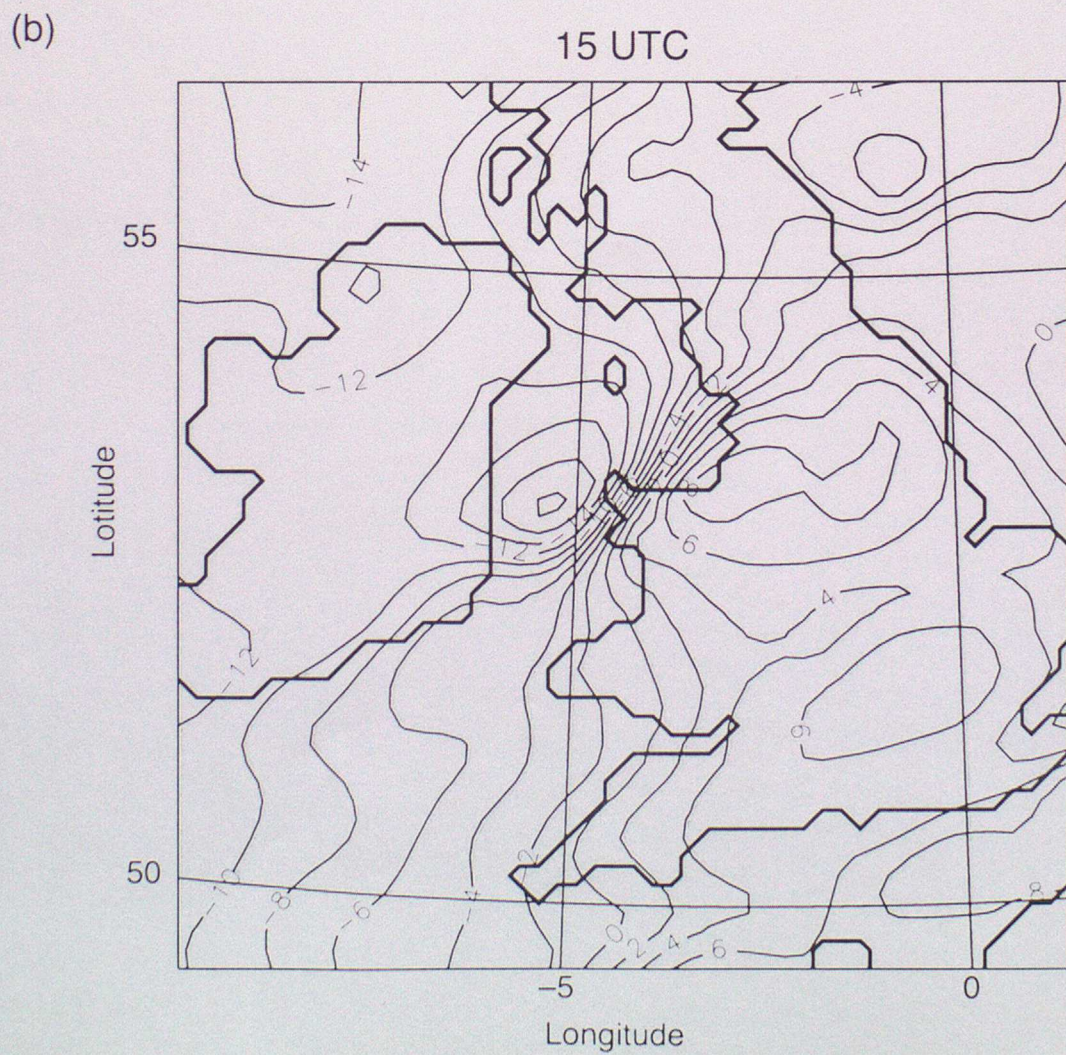
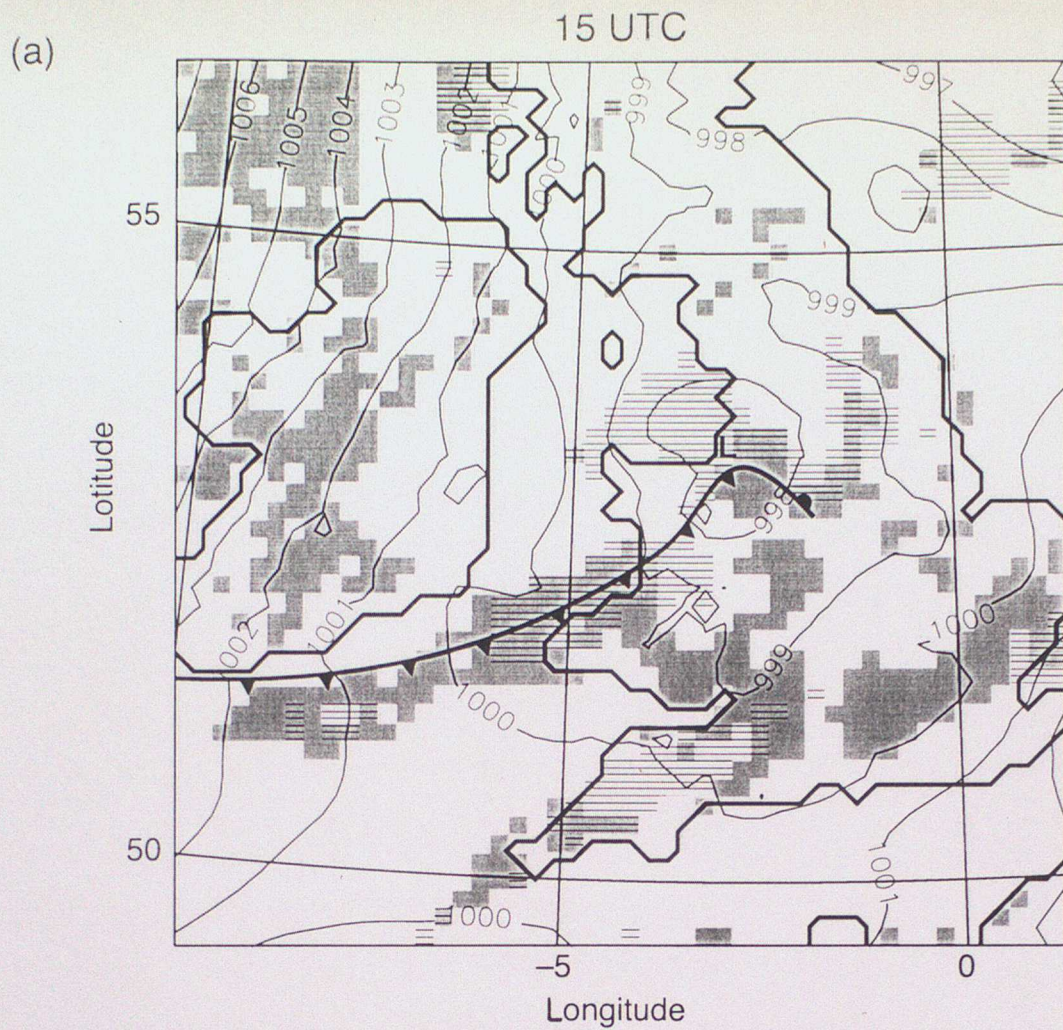
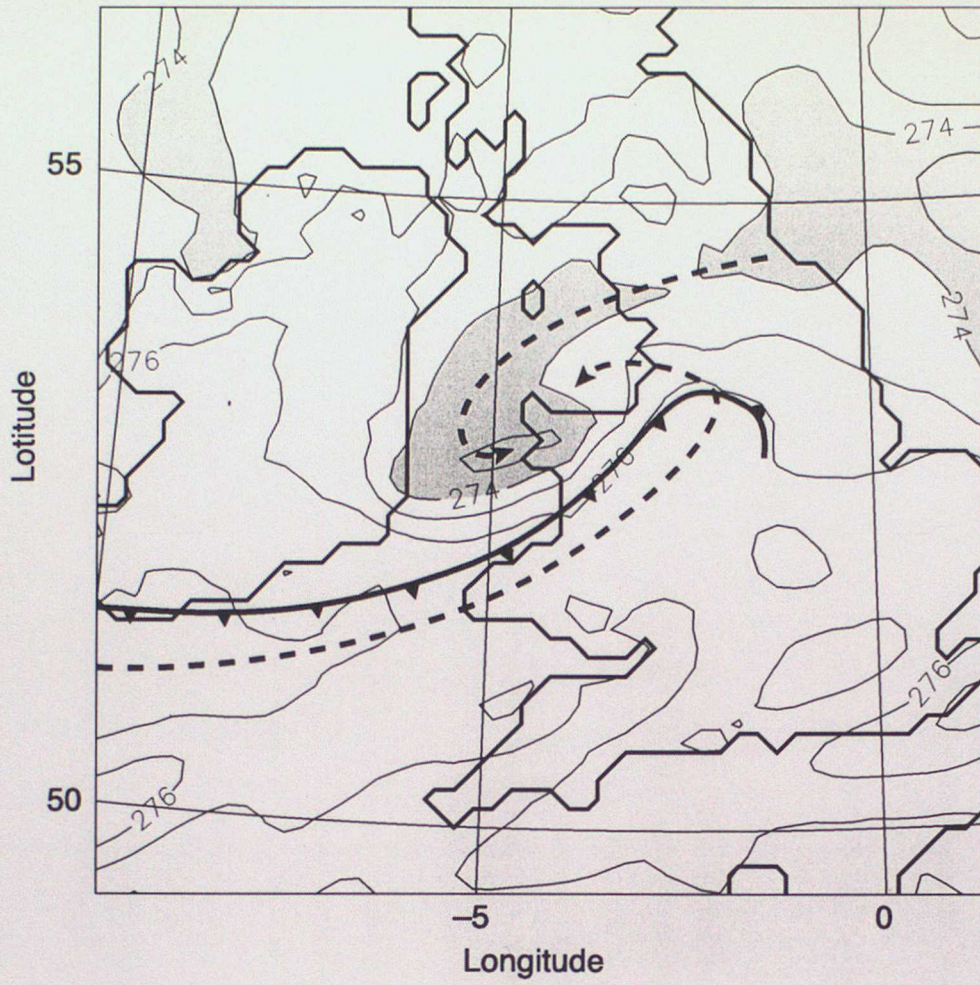


Fig 2

(c)

15 UTC



(d)

15 UTC

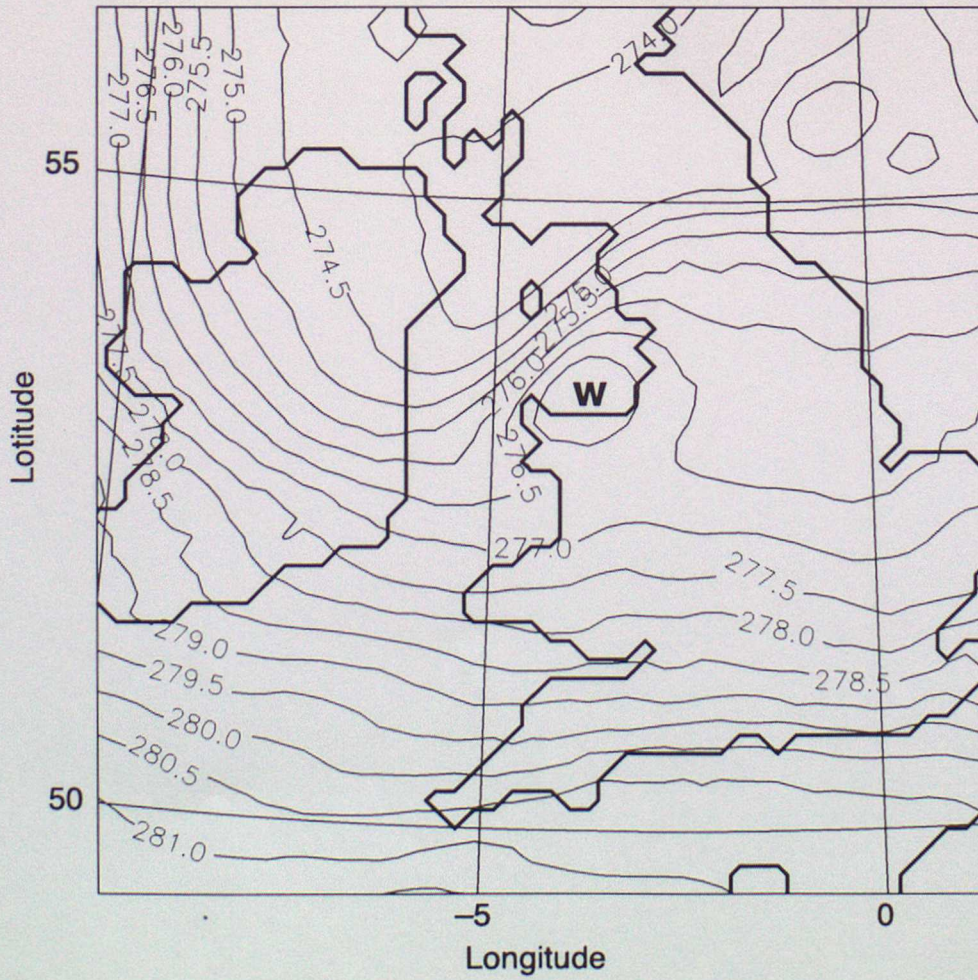
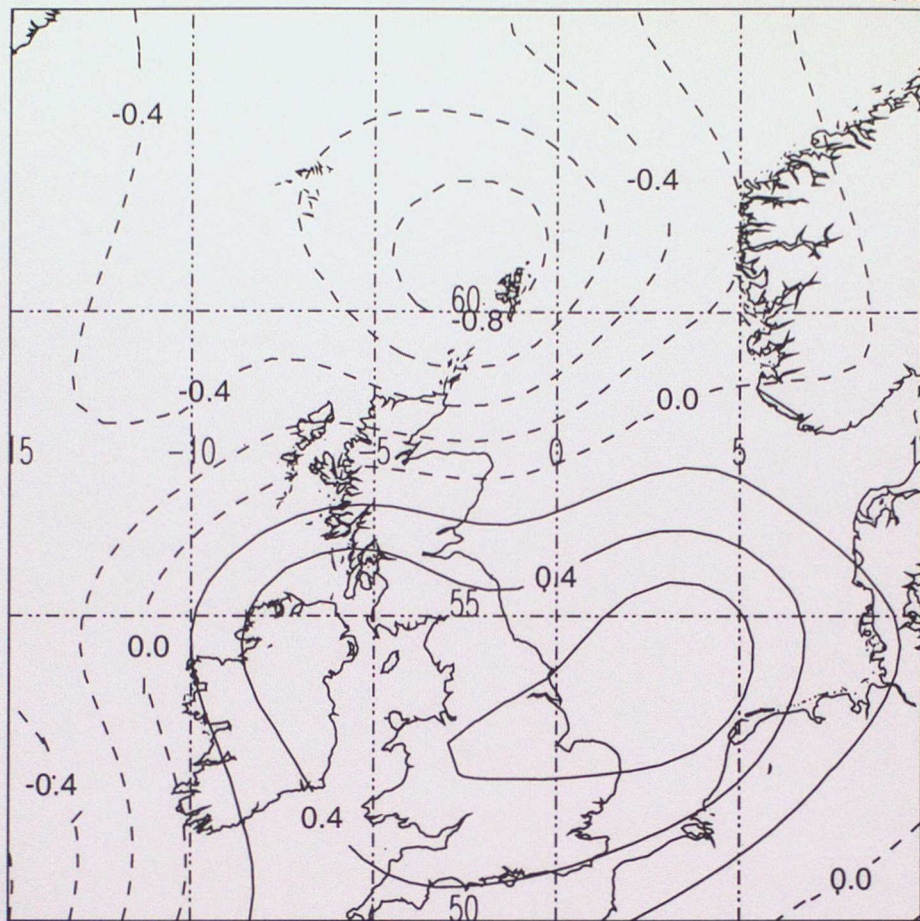


Fig 2

(a) 9UTC, 14 April 1998 upper-levels attributable  $\omega_{QG}$



(b) 9UTC, 14 April 1998 lower-levels attributable  $\omega_{QG}$

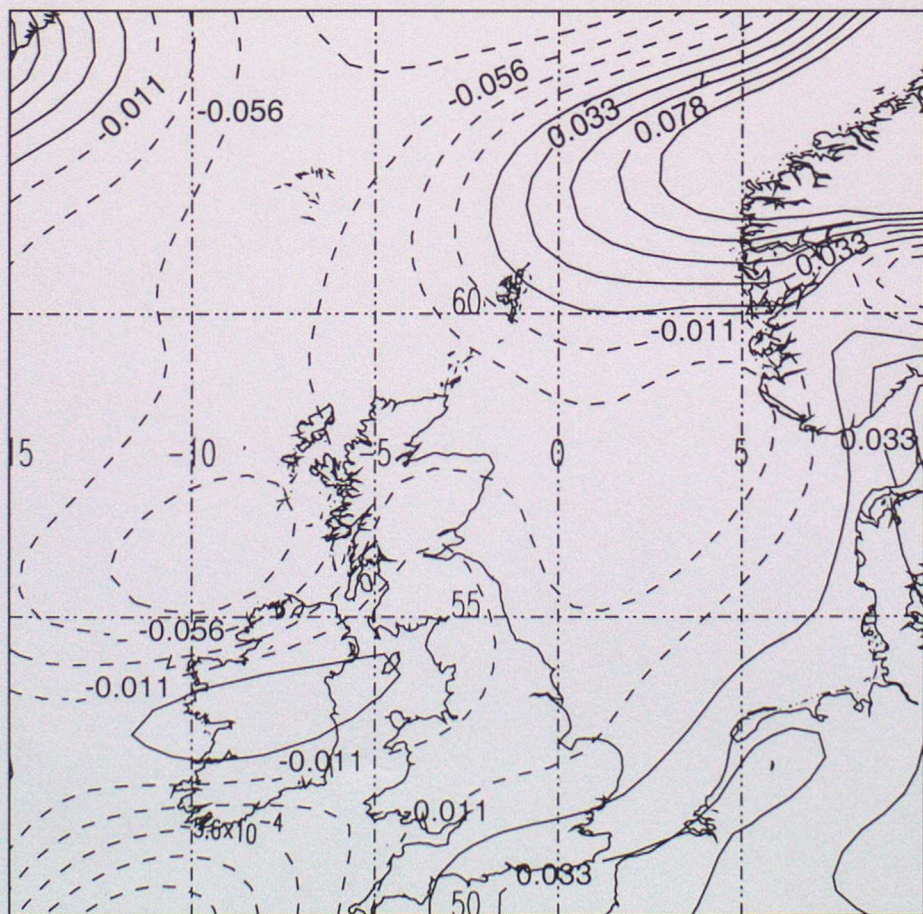


Figure 3(a) and 3(b)

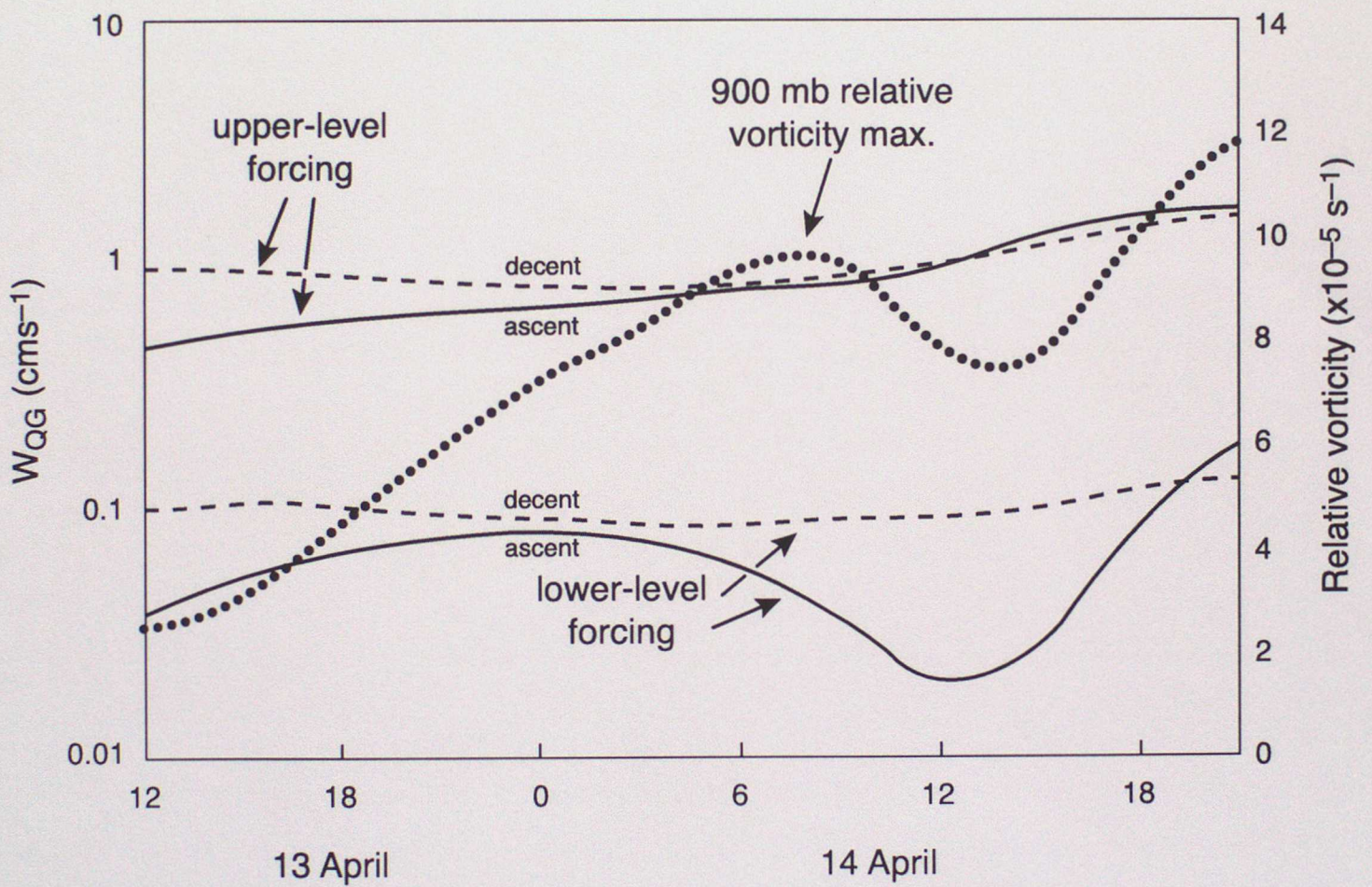
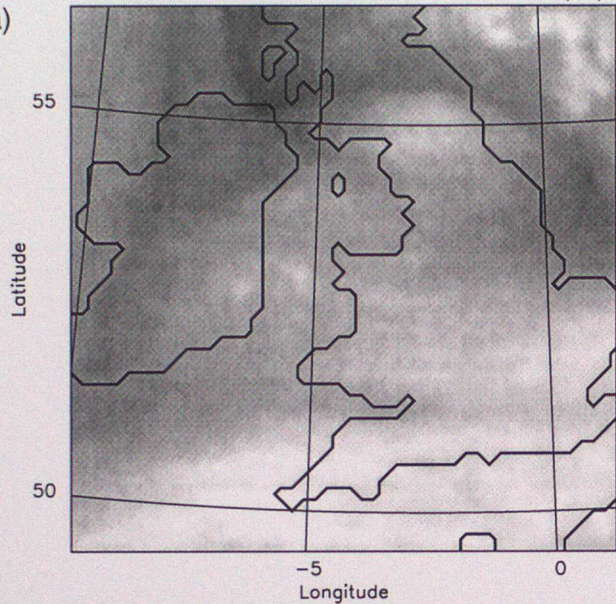
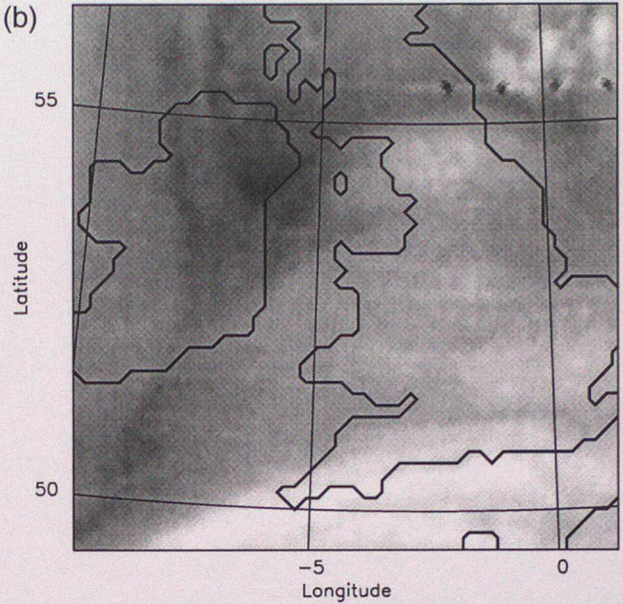


Fig 4

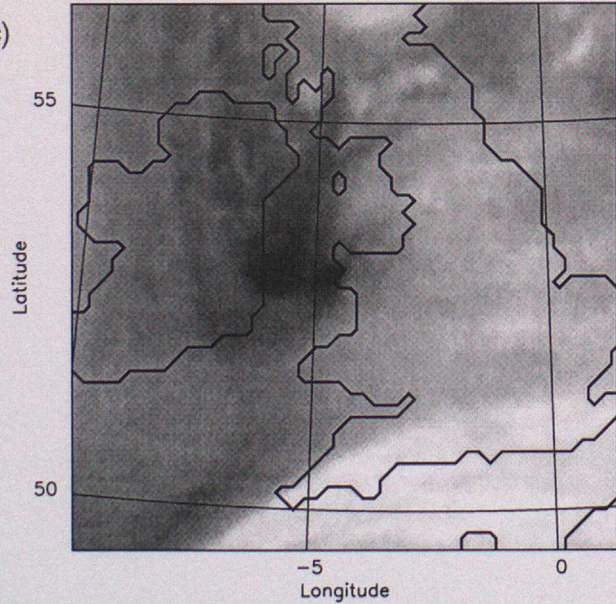
(a) WV Meteosat Satellite Data at 09:30 on 14/4/98



(b) WV Meteosat Satellite Data at 12:30 on 14/4/98



(c) WV Meteosat Satellite Data at 15:30 on 14/4/98



(d) WV Meteosat Satellite Data at 18:30 on 14/4/98

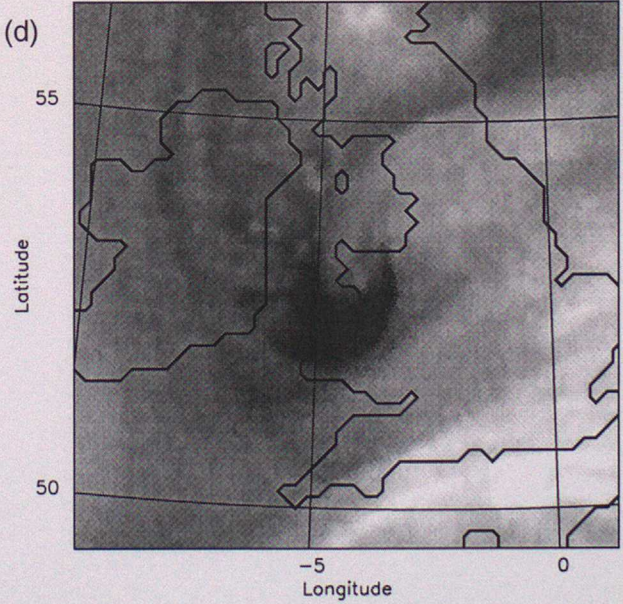


Fig. 5

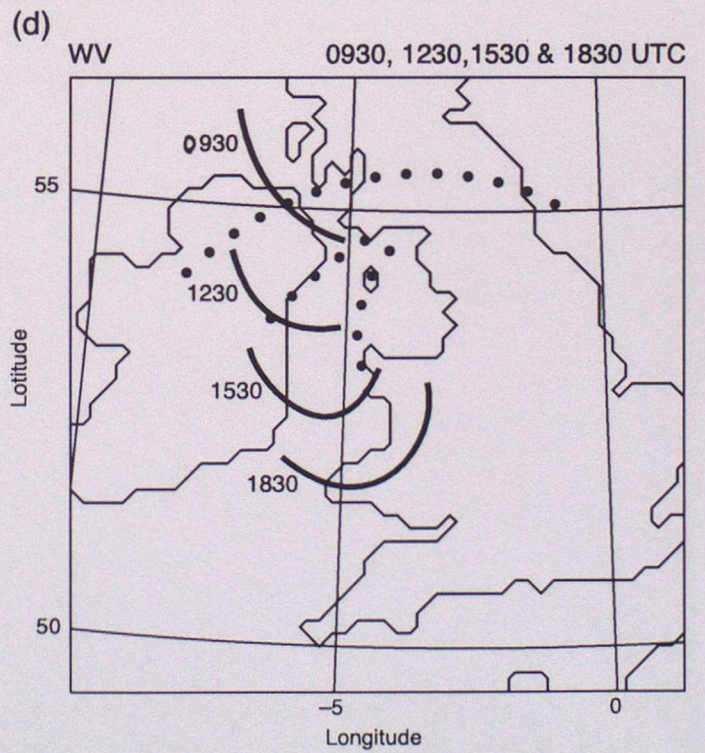
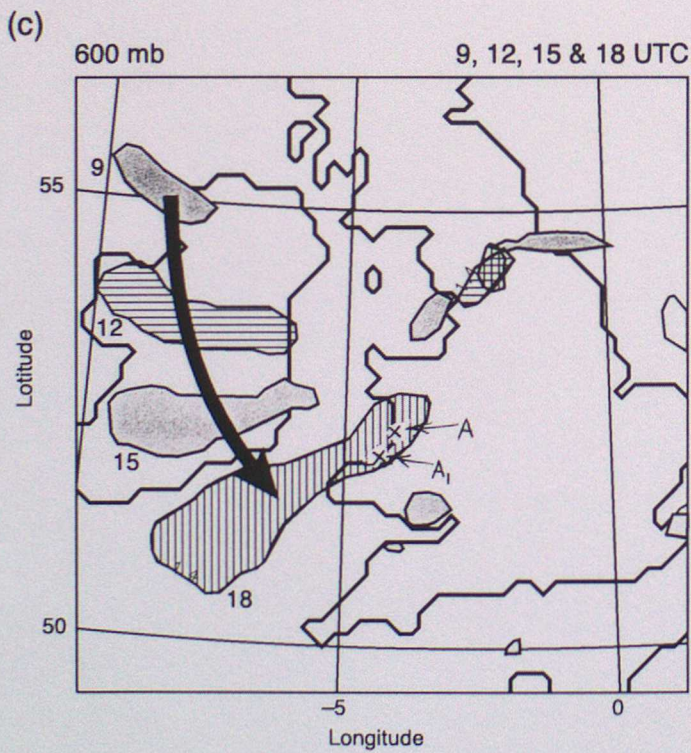
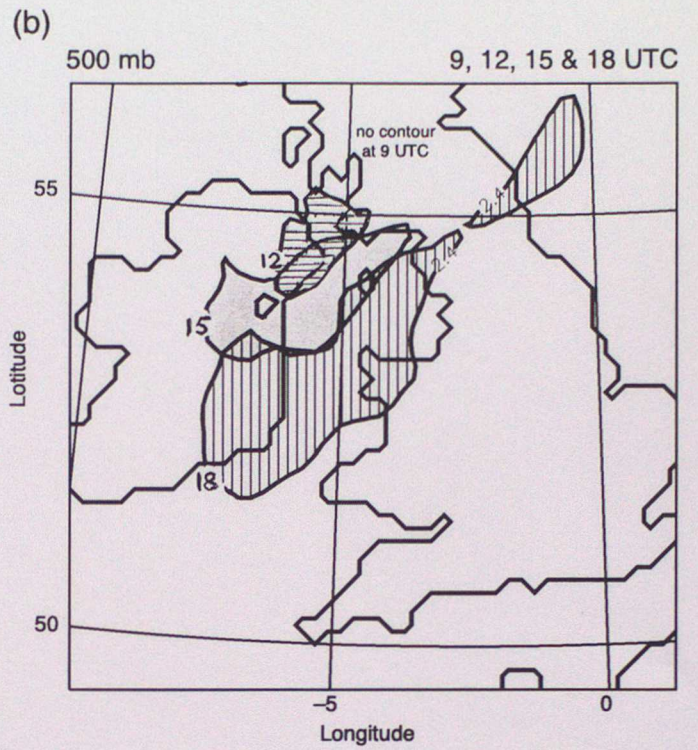
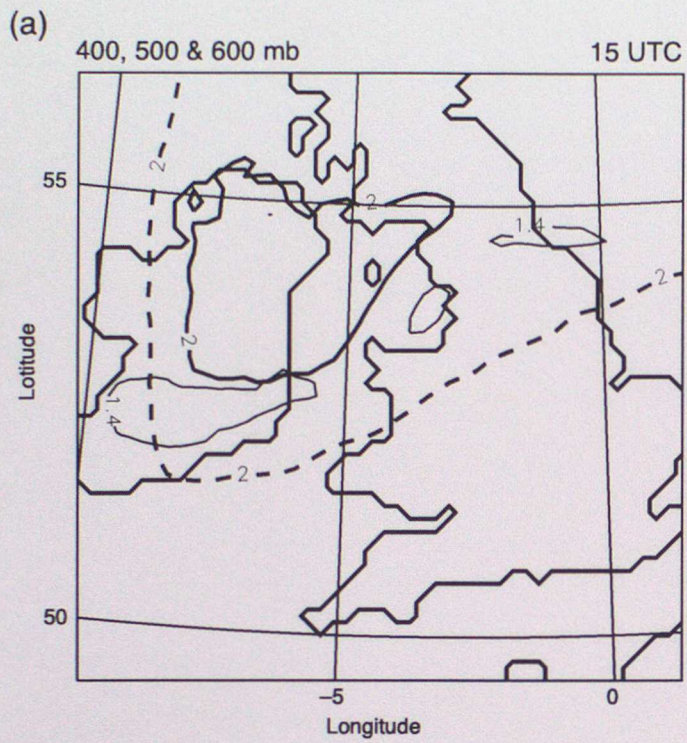
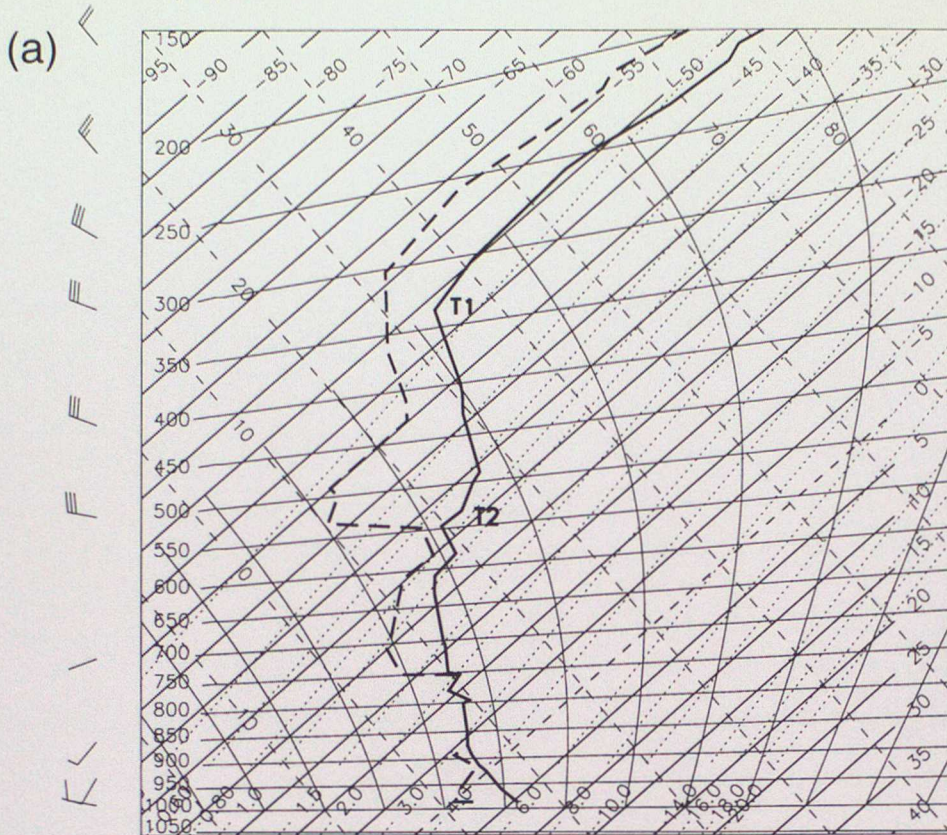


Fig 6

Aberporth Radiosonde  
14/04/98 12Z



Aberporth Radiosonde  
14/04/98 18Z

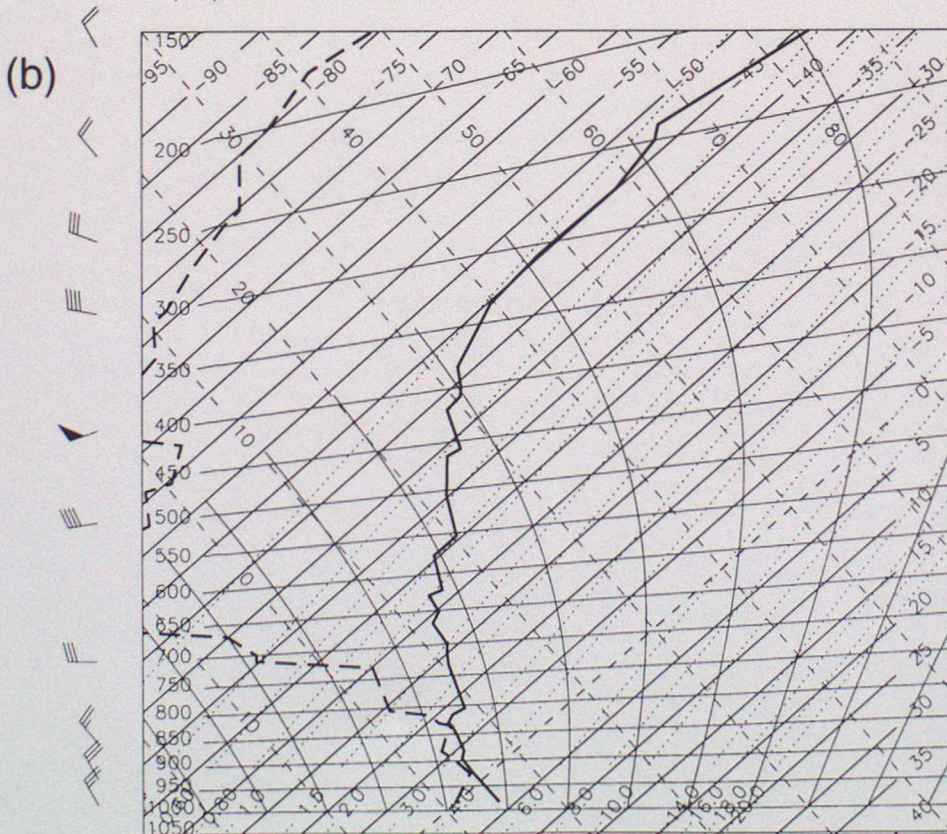
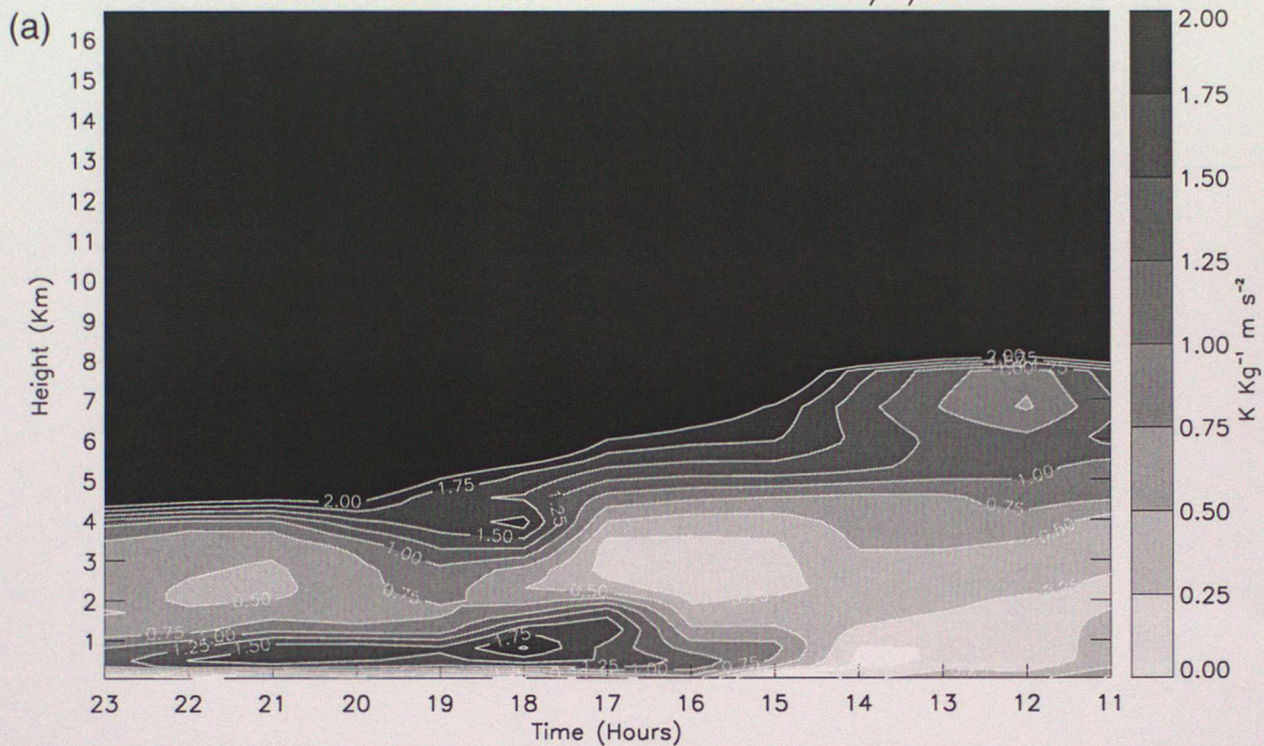


Fig. 7

Time-Height Profile of Dry PV  
Location Lat: 52.42 Lon: -4.00 on 14/4/98



Time-Height Profile of Relative Humidity (ice)  
Location Lat: 52.42 Lon: -4.00 on 14/4/98

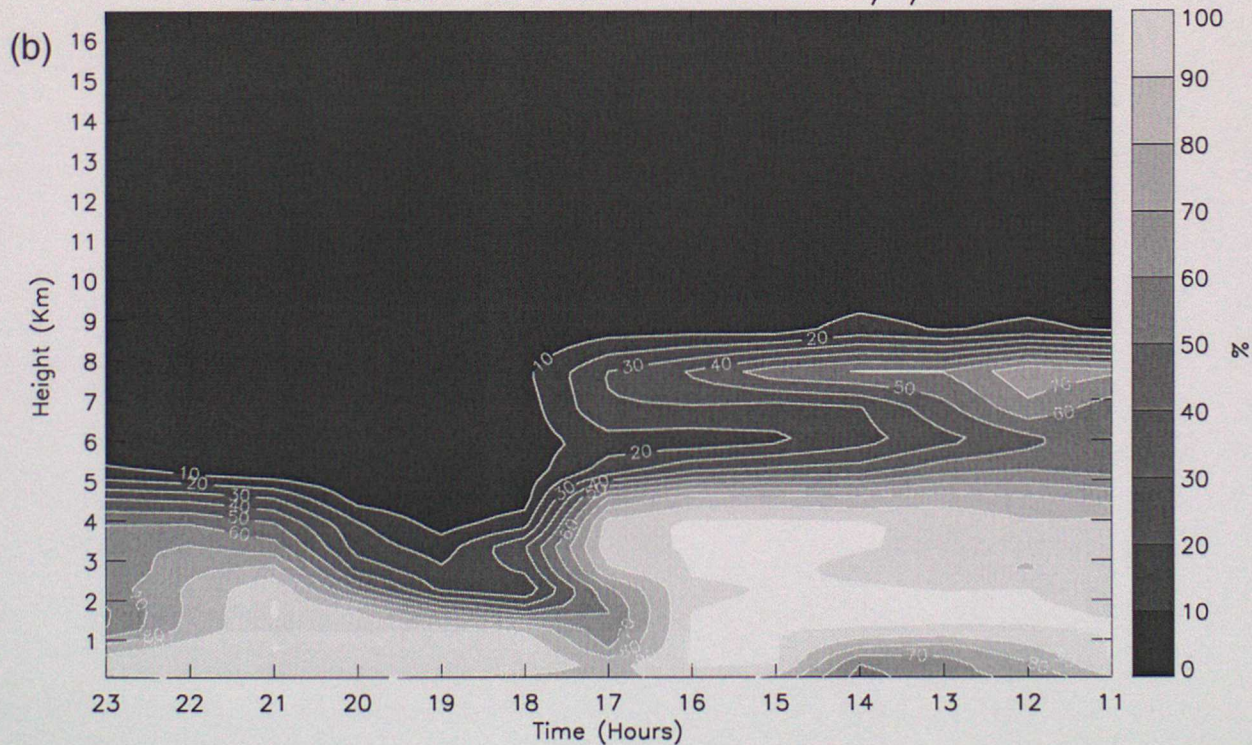


Fig. 8

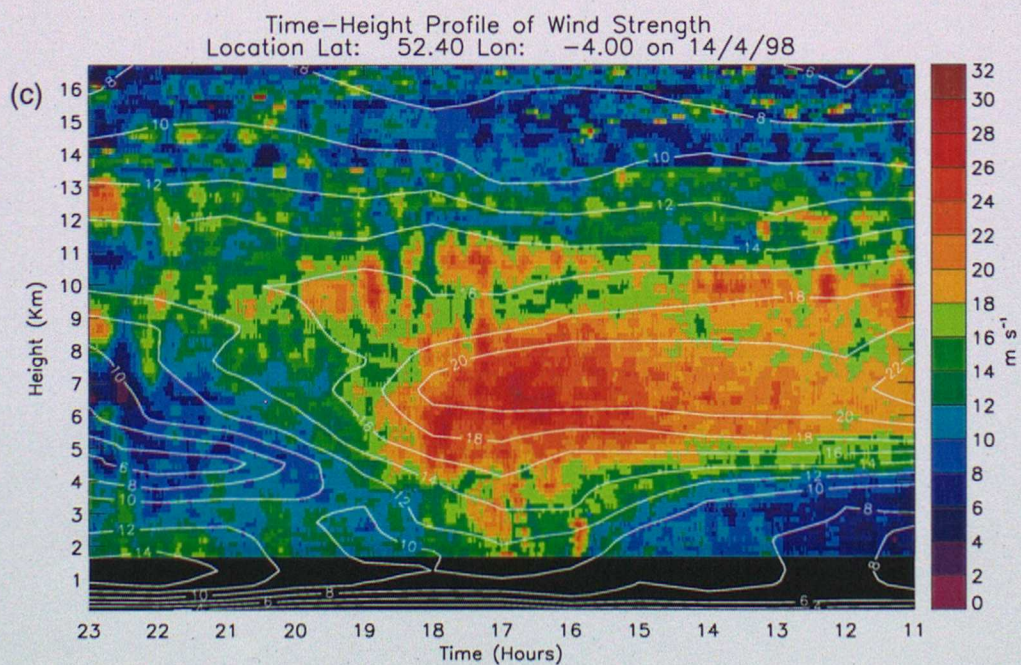
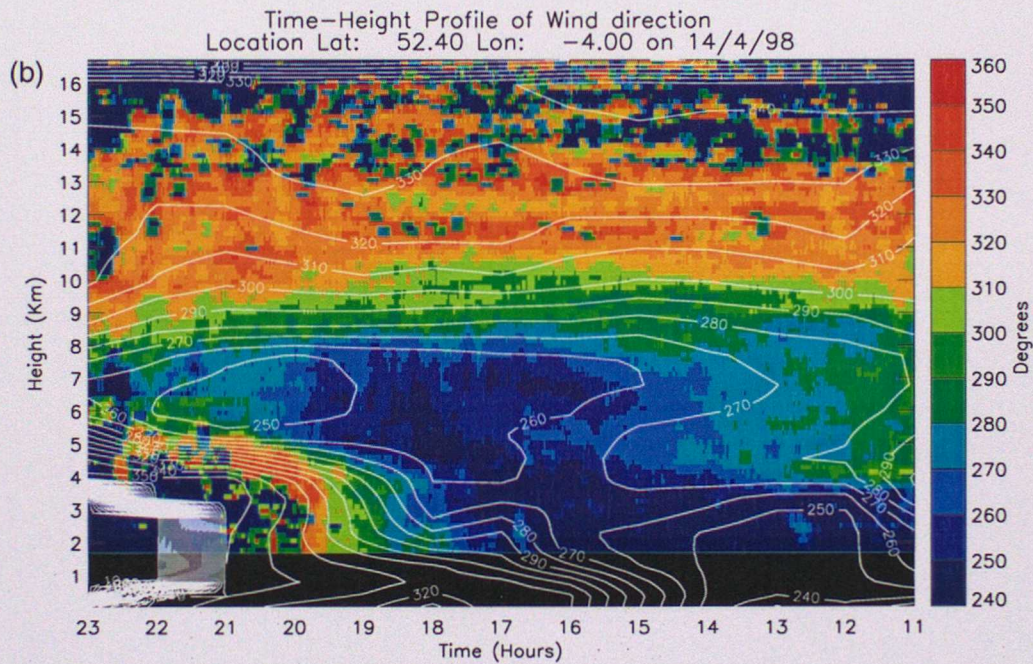
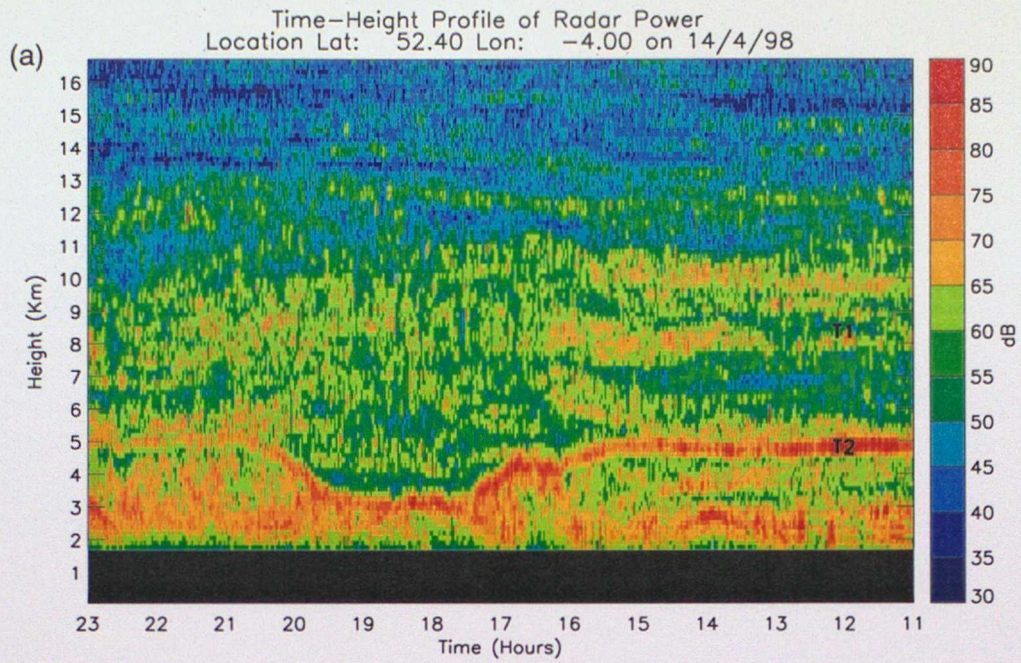


Fig. 9

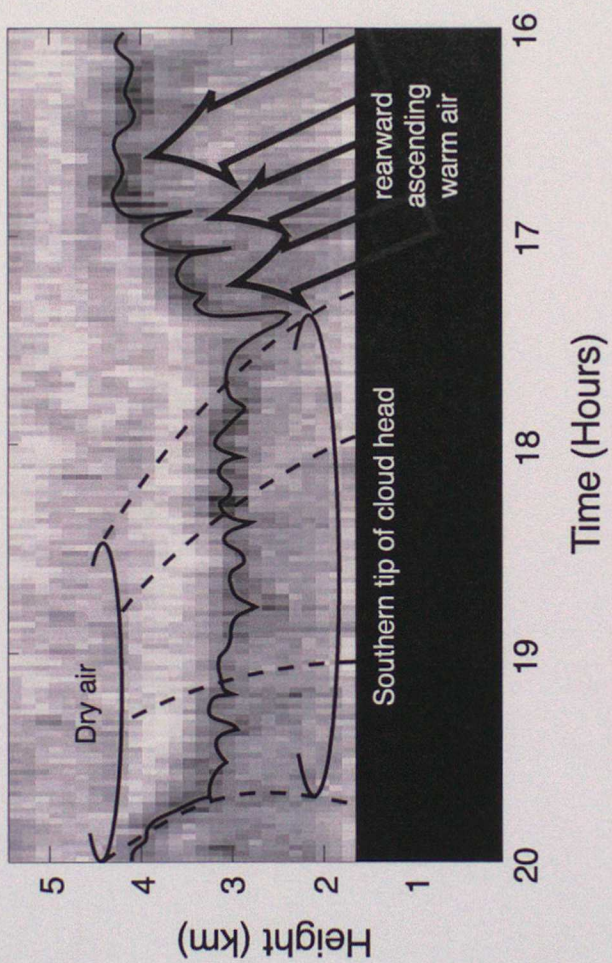


Fig 10

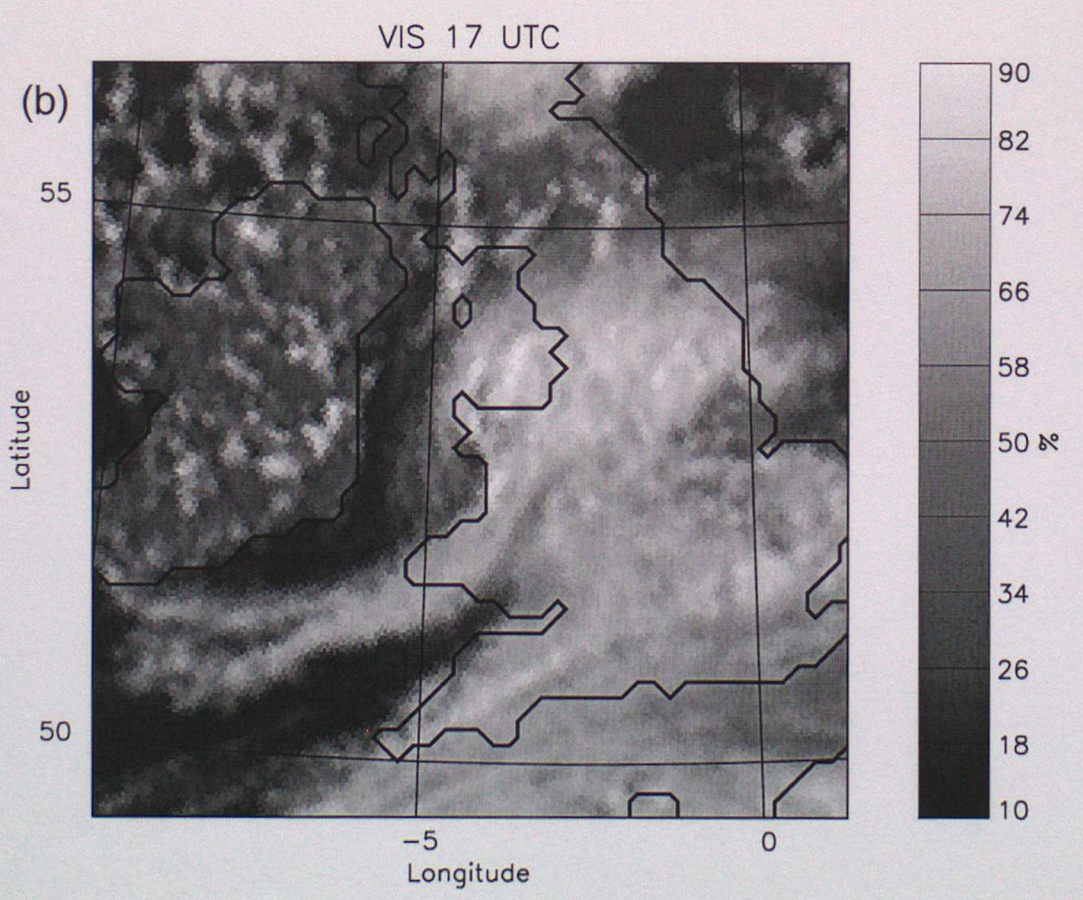
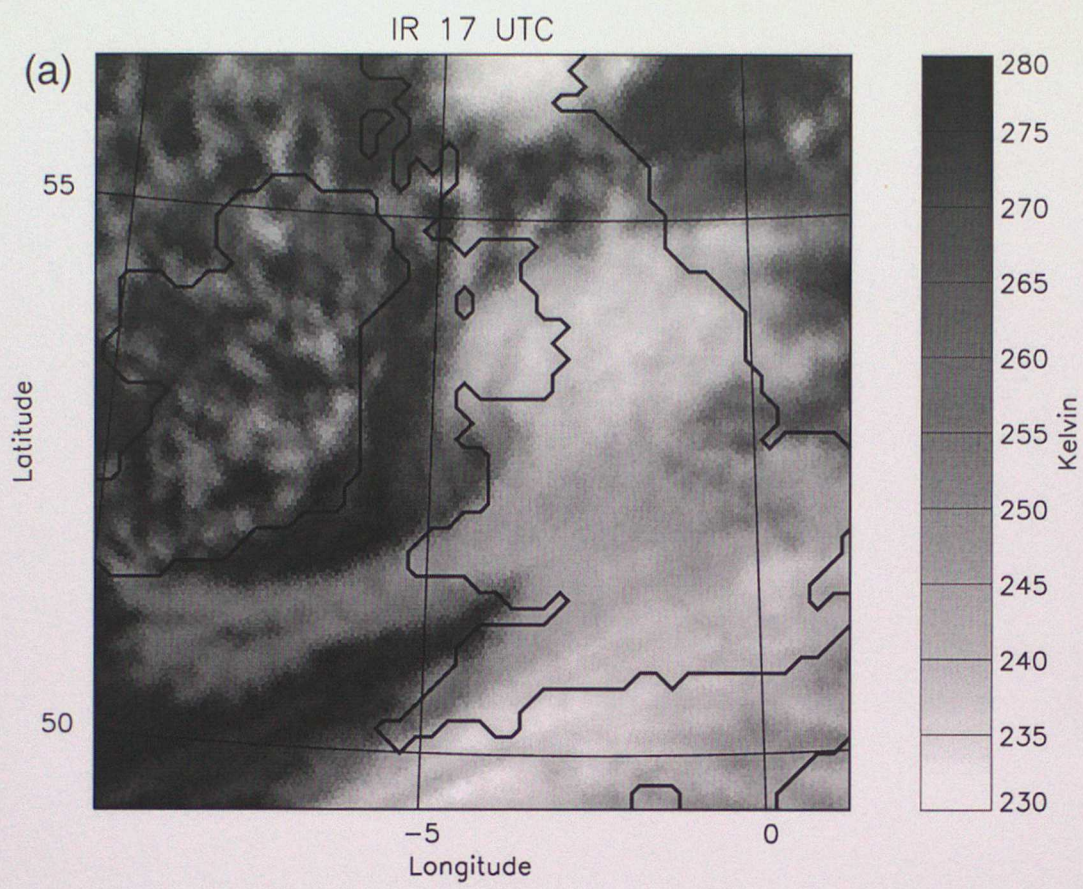


Fig. 11